Optimum Space Vector Computation Technique for Direct Power Control

Jose A. Restrepo, *Member, IEEE*, Jose M. Aller, Julio C. Viola, Alexander Bueno, and Thomas G. Habetler, *Fellow, IEEE*

***Abstract*—This study presents an efficient control technique for computing the optimum space-vector voltage in power converters. The presented optimized direct power control (ODPC) provides a closed-form formula for the converter space-vector voltage, which, based on Lagrange operators for the optimum trajectory, provides the commanded complex apparent power. The voltage required by the ODPC is obtained with a standard modulation that synthesizes the mean value required during the control cycle. The converter's performance using the ODPC algorithm improves over existing DPC-based algorithms that use constrained optimization, such as preselected space vectors or switching tables, by providing a further harmonic in content reduction, lower computational requirements, and faster time response to changes in active and reactive power commands. The use of the ODPC results in an almost instantaneous active and reactive power reference tracking, allowing for full power inversion in less than 1.0 ms under constant switching operation. Simulation results and experimental verifications are presented to validate the advantages of the proposed control algorithm. The scope of applications of this technique is those that require low harmonic impact on the ac power supply and for power quality improvement in general.**

***Index Terms*—Active filters, power control, power quality, predictive control, reactive power control.**

NOMENCLATURE

$\boldsymbol{s}$	Instantaneous apparent power.
p, q	Instantaneous active and reactive power.
ω	Supply frequency.
$\boldsymbol{v}_s, \boldsymbol{i}_s$	Instantaneous voltage and current supply space vectors.
$\boldsymbol{v}_r$	Instantaneous rectifier voltage space vector.
$\hat{\boldsymbol{v}}_s, \hat{\boldsymbol{i}}_s$	Estimated voltage and current supply vectors.
v_{sa}, v_{sb}, v_{sc}	Power source voltages.
v_{ra}, v_{rb}, v_{rc}	Mean rectifier voltages.
i_{sa}, i_{sb}, i_{sc}	Power source currents.
L, R, C	Converter's inductance, resistance, and capacitance.
L_{sc}	Per phase supply's short-circuit inductance.
$\hat{L}, \hat{R}$	Estimated inductance and resistance.
S_a, S_b, S_c	Phase a, b and c rectifier's switches states.
D_a, D_b, D_c	Duty cycle a, b and c for the converter's switches.
T_s	Sampling period.
$\Delta p_0, \Delta q_0$	Change in active and reactive power for a zero converter voltage.
ϵ_p, ϵ_q	Active and reactive power errors.
J	Cost function (Lagrange function).

Manuscript received September 29, 2008; revised December 9, 2008. Current version published June 10, 2009. Recommended for publication by Associate Editor J. R. Espinoza.

J. A. Restrepo and J. C. Viola are with the Departmento de Electrónica y Circuitos, Universidad Simón Bolívar, Caracas, Venezuela (e-mail: restrepo@usb.ve; jcviola@usb.ve).

J. M. Aller and A. Bueno are with the Departamento de Conversión y Transporte de Energía, Universidad Simón Bolívar, Caracas, Venezuela (e-mail: jaller@usb.ve; bueno@usb.ve).

T. G. Habetler is with the School of Electrical and Computer Engineering, Georgia Institute of Technology, Atlanta, GA 30332 USA (e-mail: thabetler@ee.gatech.edu).

Color versions of one or more of the figures in this paper are available online at http://ieeexplore.ieee.org.

Digital Object Identifier 10.1109/TPEL.2009.2014953

I. INTRODUCTION

THE WIDESPREAD use of ac to dc converters and the requirement of low harmonic impact and high power factor in modern industrial applications has drawn attention to the use of special passive [1] or hybrid topologies [2], and to a widespread variety of active converters [3]–[20]. Nowadays, apart from the main function of the converter, existing regulations impose an additional requirement of good power quality [21], [22]. Several techniques have been used in the control of these converters [3], each with their own advantages and disadvantages. The control techniques for power converters can be roughly classified in [4]: direct sinusoidal control of the impressed currents in the converter [5]–[7], [23], voltage-oriented control [8], [9], virtual flux orientation [10]–[12], direct power control (DPC) [13], [14], and lately optimum vector selection, predictive DPC with arbitrary active and reactive power commands, and predictive DPC for unity power factor operation [15]–[20]. From these, DPC-based techniques have attracted great attention due to its high dynamic response to demands in active or reactive power. Its basic open-loop operation allows uncoupled control of active and reactive power components, low sensitivity to parameter variations, and simplicity in implementation.

The advantages of DPC are exploited in this study, to improve the control and reduce the computational burden required by the algorithm. The standard scheme for the classical DPC is shown in Fig. 1, the DPC algorithm resembles the direct torque control (DTC) algorithm used in ac machines [13], [24], as in DTC it uses a switching table, this time for direct instantaneous power control; the active and reactive power errors are fed to hysteresis comparators and their outputs, together with the system's vector phase are used to select from the switching tables the best vector for the next control cycle. Although DPC has many advantages, some disadvantages of this control technique are high ripple content in the system current, high ripple in the commanded active and reactive power, variable switching frequency, and requires a high switching frequency.

The DPC can be forced to operate at a constant frequency by using space-vector modulation (SVM) to synthesize the

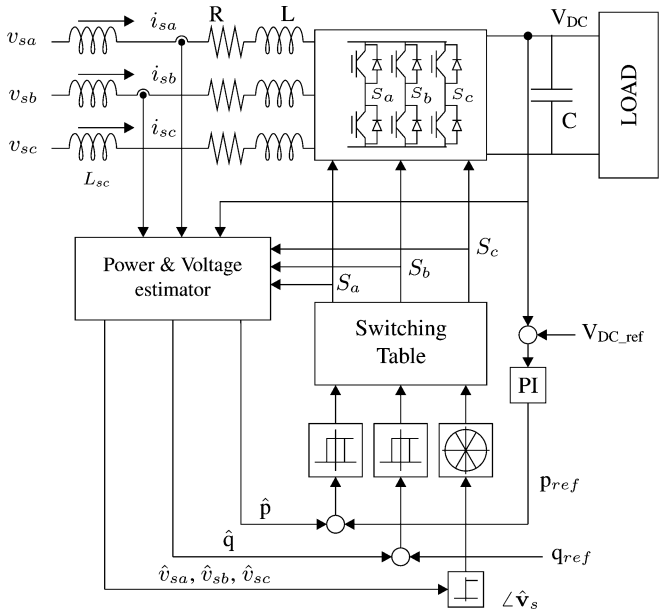

Fig. 1. Block diagram of the classical DPC.

space-vector voltage demanded by the switching table [25]. Although classical DPC uses the fix number of vectors present in this table, more vectors can be arbitrarily generated by using SVM. In this way, the ripple in current can be reduced [15], [17]–[19]. In these DPC schemes, a cost function is minimized for all the set of space-vector voltages generated by modulation, such that the predicted active and reactive power obtained from a system's model are closest to their commanded values.

This paper proposes an efficient algorithm for computing the optimum space-vector voltage that provides the commanded instantaneous active and reactive power to be drawn from the system supply. The kernel of the algorithm computes the α and β components of the converter voltage as a function of the previous voltage vector and the instantaneous active and reactive power errors, using a simple and closed-form formula obtained by forcing a quadratic cost function to zero. The proposed algorithm has been simulated and experimentally tested using extreme changes in the instantaneous active and reactive power references, showing the improved dynamic performance of the proposed controller compared with previously reported works [15], [18], [19]. A complete derivation of the closed-form formula for the proposed control algorithm is also included in this paper. Finally, an analysis and discussion of these results are presented.

II. Selection of the Best Voltage Vector for DPC

As in the classical DTC algorithm, the selection of the best voltage vector from a predefined set of discrete vectors, uses the instantaneous apparent power, computed from the following expression [26]–[28]:

$$\boldsymbol{s} = \boldsymbol{v}_s \cdot \boldsymbol{i}_s^* = (v_{s\alpha} + jv_{s\beta}) \cdot (i_{s\alpha} + ji_{s\beta})^* = p + jq \quad (1)$$

where

$$\boldsymbol{v}_s = \sqrt{\frac{2}{3}} \left(v_{sa} + v_{sb} e^{j2\pi/3} + v_{sc} e^{j4\pi/3} \right) \quad (2)$$

$$\boldsymbol{i}_s = \sqrt{\frac{2}{3}} \left(i_{sa} + i_{sb} e^{j2\pi/3} + i_{sc} e^{j4\pi/3} \right) \quad (3)$$

are the conservative power space-vector transformation [29], [30]. From Fig. 1, the converter can be modeled as

$$\boldsymbol{v}_s = \boldsymbol{v}_r + R\,\boldsymbol{i}_s + L\frac{d\boldsymbol{i}_s}{dt} \quad (4)$$

a discrete-time version of this equation is obtained by replacing the derivative with a rectangular approximation, and the estimated supply current for the next control cycle "k" becomes

$$\hat{\boldsymbol{i}}_{s\,k+1} = \boldsymbol{i}_{sk} + \Delta\hat{\boldsymbol{i}}_{sk} \quad (5)$$

where

$$\Delta\hat{\boldsymbol{i}}_{sk} = \frac{T_s}{\hat{L}} \left[\boldsymbol{v}_{sk} - \hat{\boldsymbol{v}}_{rk} - \hat{R}\,\boldsymbol{i}_{sk} \right]. \quad (6)$$

From (1), the estimated active and reactive power for the next sampling period can be written as

$$\begin{aligned} \boldsymbol{s}_{k+1} &= \boldsymbol{s}_k + \Delta\boldsymbol{s}_k \\ &= (\boldsymbol{v}_{sk} + \Delta\hat{\boldsymbol{v}}_{sk}) \cdot (\boldsymbol{i}_{sk} + \Delta\hat{\boldsymbol{i}}_{sk})^* \\ &= \boldsymbol{v}_{sk} \cdot \boldsymbol{i}_{sk}^* + \Delta\hat{\boldsymbol{v}}_{sk} \cdot \boldsymbol{i}_{sk}^* + \hat{\boldsymbol{v}}_{s\,k+1} \cdot \Delta\hat{\boldsymbol{i}}_{sk}^*. \end{aligned} \quad (7)$$

By replacing (6) in (7), the change in apparent power $\Delta\boldsymbol{s}_k = \Delta p_k + j\,\Delta q_k$ is

$$\begin{aligned} \Delta\boldsymbol{s}_k = \Delta\hat{\boldsymbol{v}}_{sk} \cdot \boldsymbol{i}_{sk}^* + \cdots \\ + \hat{\boldsymbol{v}}_{s\,k+1} \cdot \frac{T_s}{\hat{L}} \left[\boldsymbol{v}_{sk} - \hat{\boldsymbol{v}}_{rk} - \hat{R}\,\boldsymbol{i}_{sk} \right]^*. \end{aligned} \quad (8)$$

For sinusoidal voltage source power supply, the estimated $\hat{\boldsymbol{v}}_{s\,k+1}$ is obtained by rotating $\boldsymbol{v}_{sk}$ in $\Delta\theta = \omega T_s$ (in radians).

$$\hat{\boldsymbol{v}}_{s\,k+1} = \boldsymbol{v}_{sk} \cdot e^{j\omega T_s} \quad (9)$$

$$\Delta\hat{\boldsymbol{v}}_{sk} = \boldsymbol{v}_{sk} \left(e^{j\omega T_s} - 1 \right). \quad (10)$$

The instantaneous power $\boldsymbol{s}_k$ is a function of the supply voltage, and also of the rectifier voltage $\hat{\boldsymbol{v}}_{rk}$ that can be manipulated to obtain the commanded value $p_{\text{ref}} + jq_{\text{ref}}$. Defining $\Delta\boldsymbol{s}_{0k}$ as the independent vector voltage term in $\hat{\boldsymbol{v}}_{rk}$ [see (8)], the following expression can be obtained:

$$\begin{aligned} \Delta\boldsymbol{s}_{0k} &= \Delta\hat{\boldsymbol{v}}_{sk} \cdot \boldsymbol{i}_{sk}^* + \hat{\boldsymbol{v}}_{s\,k+1} \cdot \frac{T_s}{\hat{L}} \left[\boldsymbol{v}_{sk} - \hat{R}\,\boldsymbol{i}_{sk} \right]^* \\ &= \boldsymbol{v}_{sk} \cdot \boldsymbol{i}_{sk}^* \left[\left(1 - \frac{T_s\,\hat{R}}{\hat{L}} \right) e^{j\omega T_s} - 1 \right] + \frac{T_s}{\hat{L}} v_{sk}^2 \cdot e^{j\omega T_s} \end{aligned} \quad (11)$$

For a given reference in active and reactive power, the change in power for proper compensation becomes a function of the converter voltage $\hat{\boldsymbol{v}}_{rk}$. The apparent power variation $\Delta\boldsymbol{s}_k = \Delta p_k + j\,\Delta q_k$ needed to change from the actual to the demanded

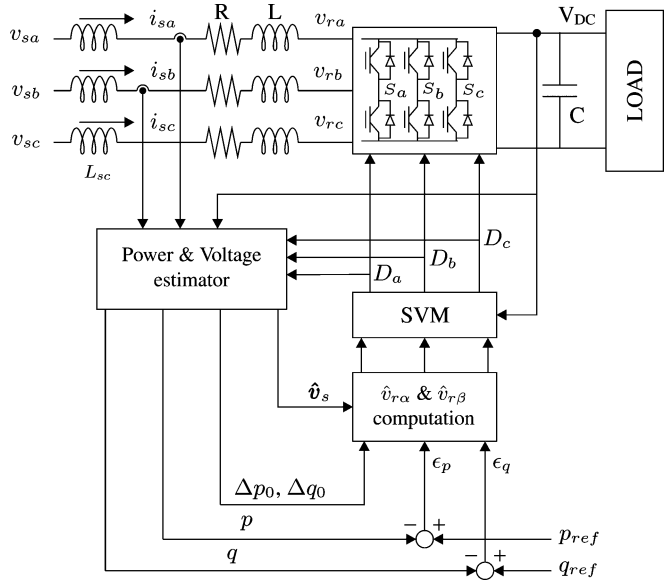

Fig. 2. Block diagram of the proposed ODPC.

value in the following sampling period, p_{ref} and q_{ref}, are given by the following expressions:

$$\Delta \boldsymbol{s}_k = \Delta \boldsymbol{s}_{0k} - \frac{T_s}{\hat{L}} \left[\hat{\boldsymbol{v}}_{s\,k+1} \cdot \hat{\boldsymbol{v}}_{rk}^* \right] \tag{12}$$

$$\begin{aligned} \boldsymbol{\epsilon}_{sk} &= \left(p_{\text{ref}\,k+1} - p_k \right) + j \left(q_{\text{ref}\,k+1} - q_k \right) \\ &= \Delta p_k + j\, \Delta q_k = \epsilon_{pk} + j \epsilon_{qk}. \end{aligned} \tag{13}$$

In the optimum vector selection scheme (OVSS) algorithm, also known as predictive DPC, a cost function is evaluated for a set of the converter voltages, and the value of this voltage providing the minimum value for the cost function is employed in the next control cycle [15], [18], [19]. In that case the cost function is the following:

$$J_k = \lambda_p (\epsilon_{pk} - \Re e[\Delta \boldsymbol{s}_k])^2 + \lambda_q (\epsilon_{qk} - \Im m[\Delta \boldsymbol{s}_k])^2 \tag{14}$$

where λ_p and λ_q control the relative importance of the active and reactive parts in the system.

These techniques require the evaluation of the cost function for each discrete voltage vector used. Hence, the computational burden is proportional to the number of discrete voltage vectors used by the algorithm. Increasing the number of space vectors improve the resulting active and reactive power ripple but more computational time is required.

III. Optimum Converter's Voltage Vector Computation

An improvement over the OVSS explained earlier is proposed in this section. The proposed ODPC block diagram is shown in Fig. 2. As with the optimum voltage vector selection scheme, the basic idea of the algorithm is to drive the converter voltage such that the cost function (14) is minimized. However, since zero is the global minimum for the cost function, instead of testing among several candidate vectors for the best choice, the proposed technique uses a closed-form formula to compute the voltage vector required to attain this minimum. Forcing to zero the cost function (14), $J_k = 0$

$$\epsilon_k - \Delta \boldsymbol{s}_k = \boldsymbol{0}. \tag{15}$$

Replacing (12) and (13) in (15)

$$\Delta \boldsymbol{s}_{0k} - \frac{T_s}{\hat{L}} \left[\hat{\boldsymbol{v}}_{s\,k+1} \cdot \hat{\boldsymbol{v}}_{rk}^* \right] = \epsilon_{pk} + j \epsilon_{qk}. \tag{16}$$

Finally, replacing (9) into (16), the absolute optimum converter voltage $\hat{\boldsymbol{v}}_{rk}$ required to attain the commanded active and reactive power becomes

$$\hat{\boldsymbol{v}}_{rk} = \hat{v}_{rk\alpha} + j \hat{v}_{rk\beta} = \frac{\hat{L}_s}{T_s} \left[\frac{\Delta \boldsymbol{s}_{0k} - \Delta \epsilon_k}{\boldsymbol{v}_{sk} \cdot e^{j\omega T_s}} \right]^*. \tag{17}$$

This voltage is synthesized in the converter using standard SVM [31]. As with other DPC algorithms, the reactor parameters L and R are required for computing the estimated value of the power system voltages, the active and reactive power, and the update value for the converter voltage indicated in (17).

The proposed algorithm has many advantages over existing methods by providing an instantaneous correction of the active and reactive power flowing into the converter, reducing the ripple in the instantaneous power and currents, reducing the harmonic content for the current into the converter, and by reducing the computational requirement of the processor used to implement the technique. Due to the fast dynamic performance of this technique, the quality of the dc bus voltage control loop is not limited by the dynamics of the proposed power controller.

IV. Simulation and Experimental Results

The active converter was simulated by programming the modeled system described by (4) using C language running on an analog devices DSP (ADSP-21369). The differential equation used for modeling the converter is solved by using a fourth order Runge–Kutta ordinary differential equations (ODEs) integrator. The integration steps during the control cycle are obtained by simulating the operation of the modulator. The power source is simulated using ideal sinusoidal generators with zero output impedance and the simulation is simplified by using a fixed voltage at the dc link. The electrical parameters for the power circuit are shown in Table I.

The simulation is done using the following steps.

- Step 1: Variables used to model the system are initialized.
- Step 2: Values for the power supply are computed and the electrical angle is increased by ωT_s.
- Step 3: Active and reactive powers are computed using (1).
- Step 4: Estimated values for supply voltage are computed.
- Step 5: Converter's vector voltage for the next control cycle is computed.
- Step 6: Duty cycles for the rectifier are calculated using SVM equations [31].
- Step 7: The ODE for the system is executed using the SVM computed integration steps.
- Step 8: The resulting system current is stored and finishes if simulation time is up, otherwise repeat from step 2.

For the experimental test, the proposed algorithm was implemented on a custom build floating-point DSP-

TABLE I
PARAMETERS AND CONDITIONS FOR THE SIMULATIONS

Supply's short circuit inductance L_{sc}	0 to 2 mH
Reactor's resistance (R)	20 mΩ
Reactor's inductance (L)	7.0 mH
DC link capacitance (C)	1100 μF
DC link load	50-200 Ω
DC link voltage (V_{DC})	200 to 600 V
Sampling and control period (T_s)	100 μ s
Line-line voltage	208 V_{rms}
Power supply frequency (ω)	60 Hz
Sampling and switching frequency	10 kHz

(ADSP-21061-40 MHz) based test-rig. The power stage uses six 50 A, 1200 V insulated gate bipolar transistors (IGBTs) with two 2200 μF 400 V series-connected capacitors in the dc link. The input inductors have an inductance $L = 7.0$ mH; the PWM signals are provided by a motion coprocessor ADMC-201 operating at 10 kHz. The load at the dc side of the converter is a 50–200 Ω adjustable power resistor. The sampling frequency is synchronized by the motion coprocessor at the beginning of each PWM cycle. The electrical parameters for the power circuit in the experimental tests are the same to those used in the simulations, and shown in Table I.

The tests used in the simulation and later verified experimentally allow to characterize the behavior of the proposed algorithm for steady-state operation and for dynamical response during high transients in the active and reactive power references. For the experimental test, the voltage and current measurements are gathered from a digital scope, harmonic contents of currents have been measured with a commercial IEC-61000 4-30 class B power quality analyzer, while the active and reactive power are taken from the processing unit.

A. Test 1: Step Changes in p and q References

The active power reference starts at 0.7 kW and changes to 1.3 kW at $t = 0.1$ s; the reactive power reference starts at -500.0 var, at $t = 0.06$ s is changed to $+500.0$ var and at $t = 0.14$ s changes back to -500.0 var. For comparison, Fig. 3 shows three different methods applied for the active and reactive power control. Fig. 3(a) shows the results using the Noguchi's switching table [13] and Fig. 3(b) shows the same case using OVSS [32]. Fig. 3(c) and (d) shows the corresponding simulated and experimental results for the same cases after applying the proposed ODPC. The simulated active and reactive power evolution shown in Fig. 3(c) has the corresponding supply voltage and current shown in Fig. 4(a). The experimental results for this test are shown in Fig. 4(b). There is a close match between the evolution of the variables in the simulation and in the experimental test, showing in this way the validity of the theoretical prediction. As expected, the proposed ODPC method has a higher dynamical response to changes in the commanded active and reactive power than previously reported methods [18]–[20], [33], this is mainly due to the absence of internal loops as opposed to other control algorithms and a significative reduction in

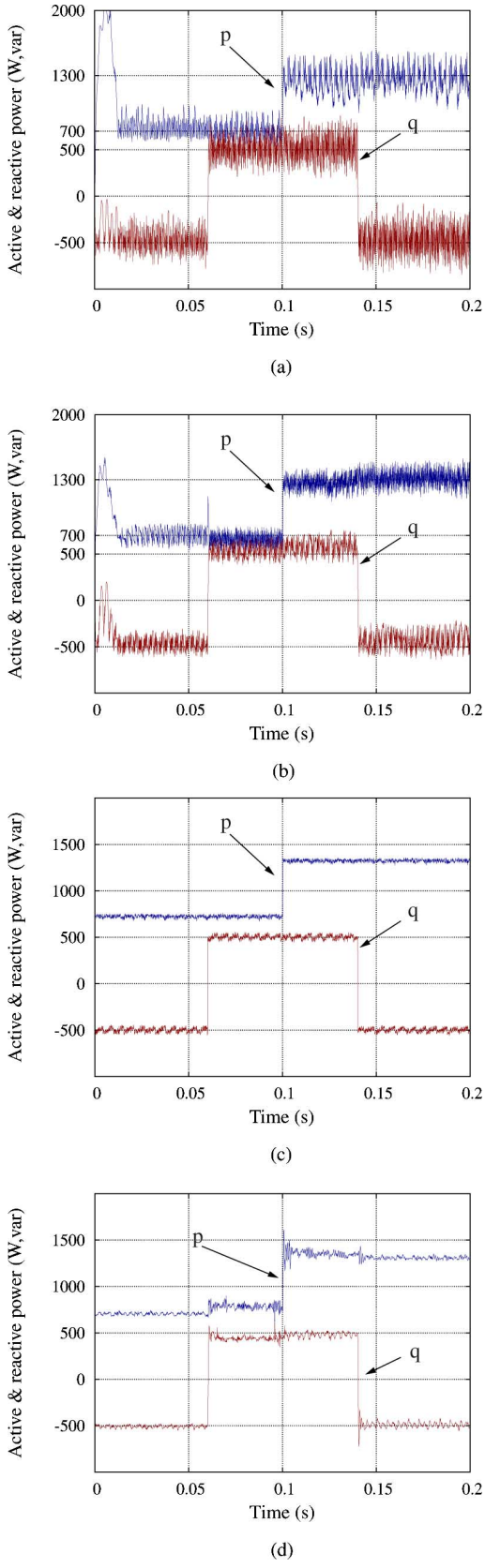

Fig. 3. Active and reactive power during test 1 using Noguchi's table and OVSS. (a) Simulated active and reactive power using Noguchi's switching table. (b) Simulated active and reactive power using OVSS. (c) Simulated active and reactive power using ODPC. (d) Experimental active and reactive power using ODPC.

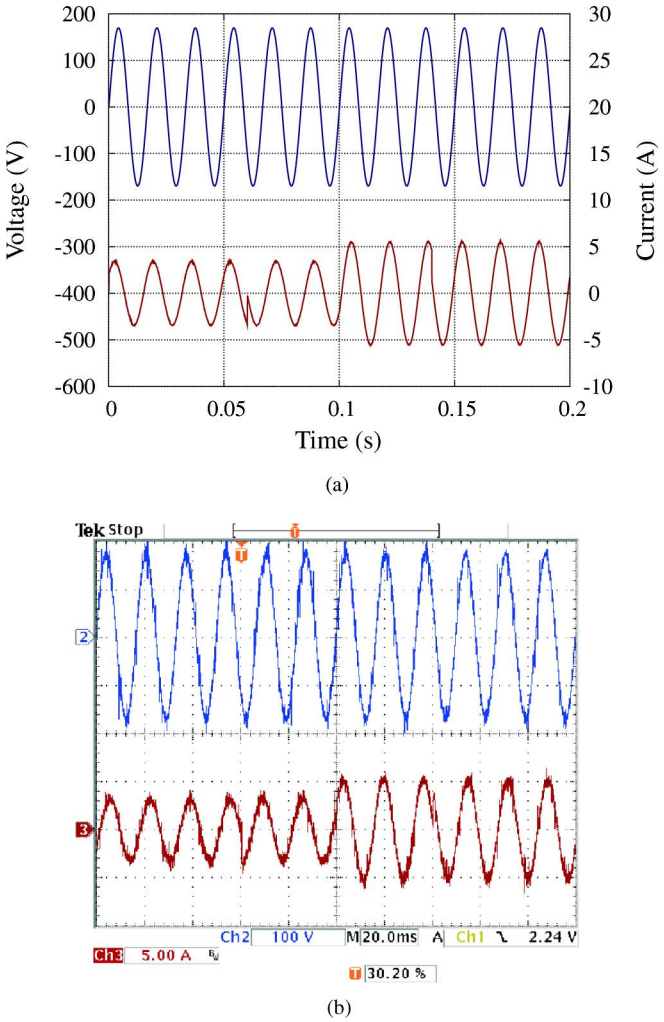

Fig. 4. Phase "a" voltage (upper trace) and current (lower trace) during test 1. (a) Simulated supply voltage and current. (b) Experimental supply voltage and current.

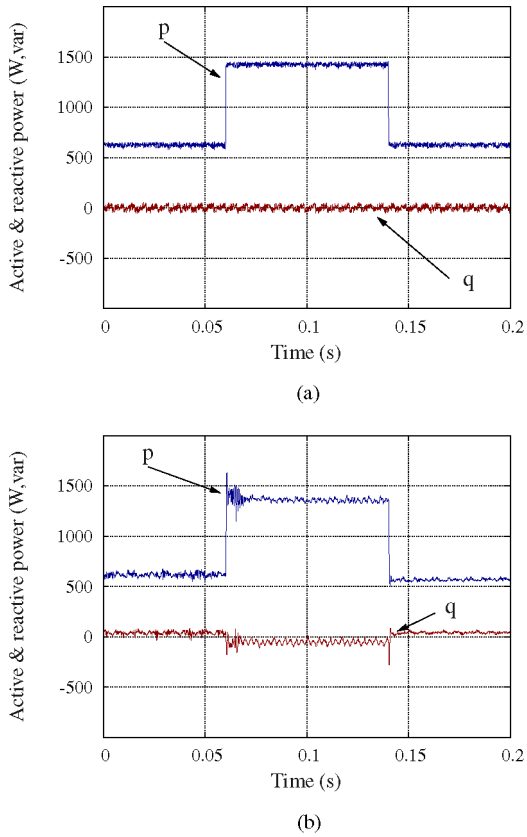

Fig. 5. Result of the active and reactive power during test 2. (a) Simulated active and reactive power. (b) Experimental active and reactive power.

the resulting active and reactive power ripple is obtained with the proposed method. Also, the result shows the converter capability to perform an independent control of the active and reactive power flow. The experimental result presented in Fig. 3(d) shows a small coupling between the active and reactive components, due to parameter mismatch and to some approximations in the experimental implementation.

B. Test 2: Step Changes in Active Power at Unity Power Factor

In this test, the system is operated at unity power factor and its response to a step change in the active power command is studied. The active power reference starts at 0.6 kW, at $t = 0.06$ s changes to 1.4 kW, and at $t = 0.14$ s is changed back to 0.6 kW. The reactive power reference is maintained at 0.0 var during this test. Fig. 5 shows the operation for active power change during operation at unit power factor. The reactive power is basically unaffected by the change in command in the active power. Fig. 6 shows the evolution of power supply voltage and current, the supply current increases its magnitude in response to the increase in active power demand, as expected, while maintaining its relative phase with the power supply voltage. A small perturbation in the resulting reactive power is also observed in this test due to cross coupling and parameter mismatch. A close match between simulation and experimental test has also been obtained in this case.

C. Test 3: Effect of Model Parameters Detuning

In this test, the imprecise model values for resistance and inductance used by the algorithm is investigated. The active power reference is maintained at 1.0 kW and the reactive power reference is maintained at -500.0 var for a parameter mismatch between -30% and $+60\%$. Variation of the resistance model parameter between 0% and 300% of its real value in the circuit is not noticeable in the resulting p- and q-values, due mainly to the high quality factor of the reactors at 60 Hz, larger than $Q = 132$, used in the test-rig. The control algorithm is executed initially with a -30% inductance mismatch; at $t = 0.05$ s, the algorithm uses a matching value for the inductance; at $t = 0.1$ s, the estimated inductance is increased in 30%; and finally, at $t = 0.15$ s, the algorithm uses a $+60$ % inductance mismatch. Fig. 7 shows the effect of inductance mismatch on the active and reactive power ripple. The active and reactive power ripple caused by a negative mismatch is less important than that of the positive mismatch, the average value of active and reactive power is maintained independently of this mismatch, and for positive mismatch, the behavior of the controller resembles

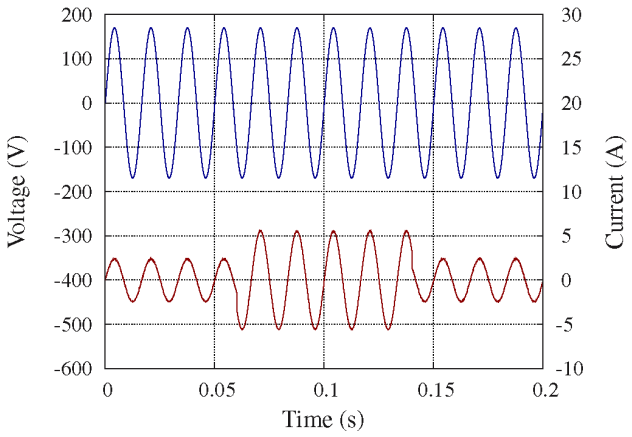

(a)

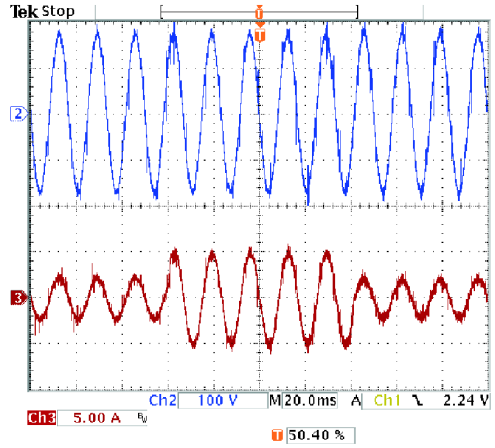

(b)

Fig. 6. Phase "a" voltage (upper trace) and current (lower trace) during test 2. (a) Simulated supply voltage and current. (b) Experimental supply voltage and current.

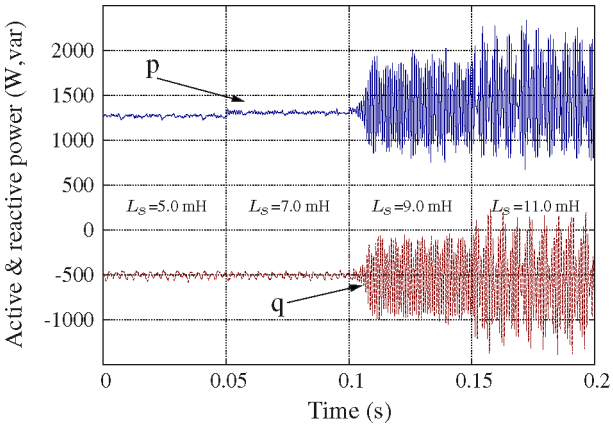

Fig. 7. Active and reactive power for changes in the estimated inductance (Test 3).

that of the classical DPC. A large positive mismatch operation has low effect over dc links, similar to the one observed using the classic DPC algorithm. For practical applications, this mismatch in parameters is often not a problem because the reactor's parameters can be easily obtained and do not show substantial changes during normal operation.

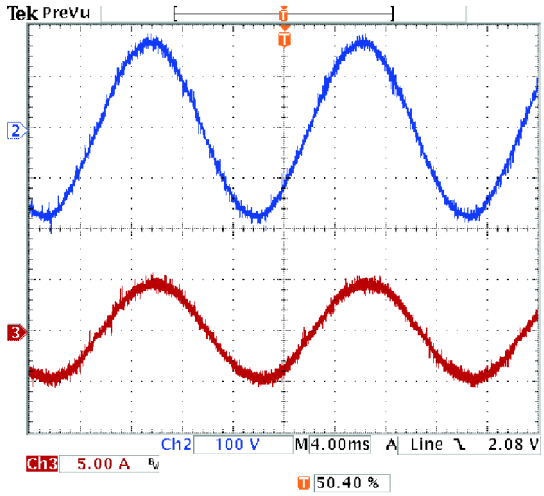

(a)

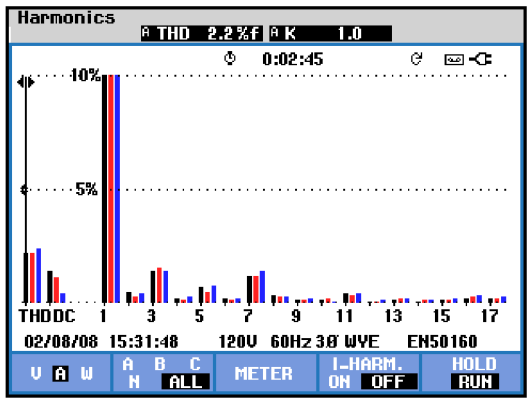

(b)

Fig. 8. Converter operation consuming active power using the proposed control scheme. (a) Phase "a" voltage (upper trace) and current (lower trace) supply. (b) Harmonic content of the supply currents.

D. Test 4: Harmonic Distortion Impact on the Supply

This test was performed experimentally on a stiff power supply to show the resulting current signal waveform and harmonic current content during operation in steady state at unity power factor delivering 1.4 kW, but on a weak power supply with short-circuit inductances reaching up to 30% of the converter's inductance the results are barely affected. Fig. 8 shows a total harmonic distortion (THD) of 2.2% of the fundamental and the harmonic distribution for the three phase currents. The third harmonic present in the distribution is due to a 3% imbalance in the voltage supply.

Fig. 9 shows the results during power regeneration, in this case the power command was set to −1.0 kW. Small offsets in the measuring sensors induce even harmonics, as shown in the harmonic current distribution. The THD attained in this test was 2.6% of the fundamental current.

Finally, the rectifier operation is verified for a step change in power consumption–regeneration. The dc link is operated by an independent power supply at 480 V, the reactive command is set to 0.0 var, and the active power command starts at 1.0 kW;

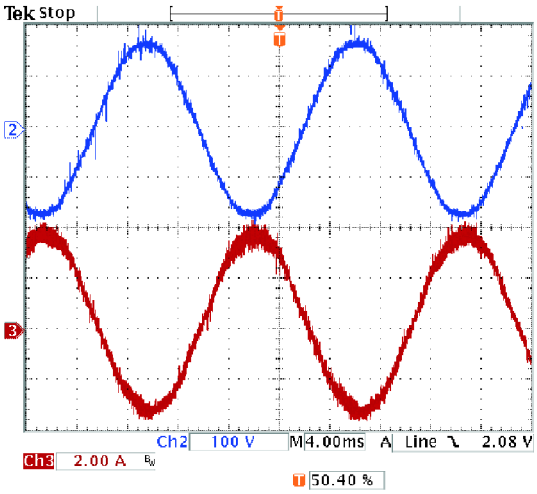

(a)

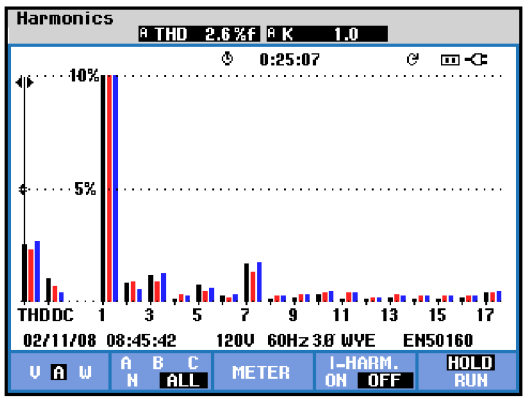

(b)

Fig. 9. Rectifier operation regenerating active power using the proposed control scheme. (a) Phase "a" voltage (upper trace) and current (lower trace) supply. (b) Harmonic content of the supply currents.

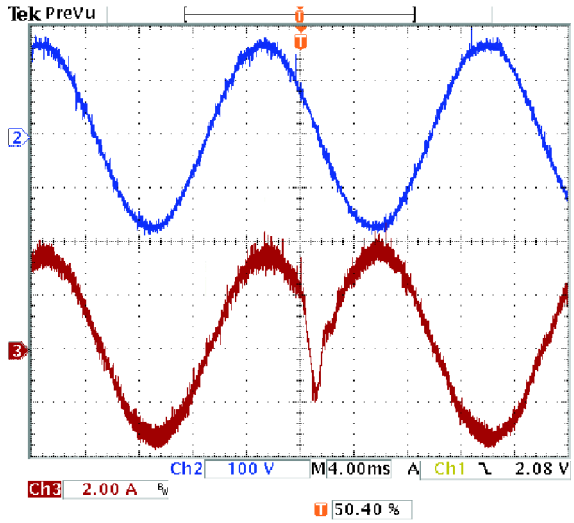

Fig. 10. Supply voltage (upper trace) and current (lower trace) during a step change from power consumption to power regeneration.

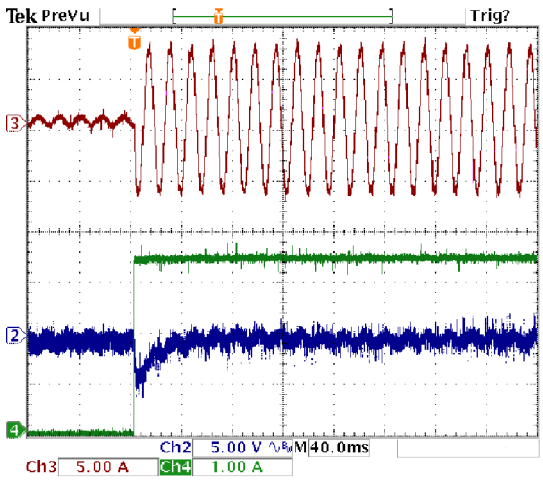

Fig. 11. DC voltage transient during a load step from zero to full load.

at $t = 0.1$ s, the active power command is changed to -1.0 kW. Fig. 10 shows that the current during the change in power flow adapts to the new operating condition in less that 1/16th of the supply cycle.

E. Test 5: DC-Link Closed-Loop Operation

This test was performed experimentally to show the transient response of the dc link during a load step from zero to full load. A predictive fuzzy controller was employed for the dc-link control loop and the experimental results are presented in Fig. 11. The upper trace shows the current in phase "a" taken from the supply. The lower part depicts the ac component in the dc link and the step change in load current. The controller is able to reestablish the dc voltage reference in less than 40 ms, and the voltage drop is about 5 V for a 350 V dc link ($\sim$1.5%). The practically instantaneous power control dynamics allows the controller in the dc-link loop to adjust its value in this short time.

V. Conclusion

The simulation and experimental results have shown that a switching strategy based on optimum rectifier space-vector voltage for DPC is a better alternative than the traditional table-based DPC algorithm and than constrained optimization used in OVSS because it provides less current ripple, faster tracking response, constant switching frequency, low harmonic injection to the supply, and robustness against model's parameter detuning or against power system's low short-circuit capacity. The processing power required by the proposed technique (ODPC) is less intensive than the one for constrained-based algorithms. Some undesirable cross coupling between the active and reactive power commands in the experimental implementation is due to parameter mismatch and some approximations in the final computation algorithm. An almost instantaneous response, limited by the control cycle period, is attained with this algorithm due to the quick change that can produce the converter in the

demanded active and reactive power. Additionally, the ODPC allows for a power reversal in less than 1.0 ms. The supply current THD obtained using this technique is smaller than those provided in recent literature for constrained-based techniques. For controlling the dc link, the limitation in transient response depends mainly on the dynamics of the external control loop and not due the ODPC proposed in this study.

REFERENCES

[1] F. J. Chivite-Zabalza, A. J. Forsyth, and D. R. Trainer, "A simple, passive 24-pulse AC–DC converter with inherent load balancing," *IEEE Trans. Power Electron.*, vol. 21, no. 2, pp. 430–439, Mar. 2006.

[2] M. E. Villablanca, J. I. Nadal, and M. A. Bravo, "A 12-pulse AC–DC rectifier with high-quality input/output waveforms," *IEEE Trans. Power Electron.*, vol. 22, no. 5, pp. 1875–1881, Sep. 2007.

[3] J. R. Rodriguez, J. W. Dixon, J. R. Espinoza, J. Pontt, and P. Lezana, "PWM regenerative rectifiers: State of the art," *IEEE Trans. Ind. Electron.*, vol. 52, no. 1, pp. 5–22, Feb. 2005.

[4] M. Malinowski, M. P. Kazmierkowski, and A. M. Trzynadlowski, "A comparative study of control techniques for PWM rectifiers in AC adjustable speed drives," *IEEE Trans. Power Electron.*, vol. 18, no. 6, pp. 1390–1396, Nov. 2003.

[5] J. W. Dixon and B.-T. Ooi, "Indirect current control of a unity power factor sinusoidal current boost type three-phase rectifier," *IEEE Trans. Ind. Electron.*, vol. 35, no. 4, pp. 508–515, Nov. 1988.

[6] R. Wu, S. B. Dewan, and G. R. Slemon, "Analysis of a PWM AC to DC voltage source converter under the predicted current control with a fixed switching frequency," *IEEE Trans. Ind. Appl.*, vol. 27, no. 4, pp. 756–764, Jul./Aug. 1991.

[7] V. Blasko and V. Kaura, "A new mathematical model and control of a three-phase AC-DC voltage source converter," *IEEE Trans. Power Electron.*, vol. 12, no. 1, pp. 116–123, Jan. 1997.

[8] T. G. Habetler, "A space vector-based rectifier regulator for AC/DC/AC converters," *IEEE Trans. Power Electron.*, vol. 8, no. 1, pp. 30–36, Jan. 1993.

[9] B.-H. Kwon, J.-H. Youm, and J.-W. Lim, "A line-voltage-sensorless synchronous rectifier," *IEEE Trans. Power Electron.*, vol. 14, no. 5, pp. 966–972, Sep. 1999.

[10] J. L. Duarte, A. Van Zwam, C. Wijnands, and A. Vandenput, "Reference frames fit for controlling PWM rectifiers," *IEEE Trans. Ind. Electron.*, vol. 46, no. 3, pp. 628–630, Jun. 1999.

[11] M. Malinowski, M. P. Kazmierkowski, S. Hansen, F. Blaabjerg, and G. D. Marques, "Virtual-flux-based direct power control of three-phase PWM rectifiers," *IEEE Trans. Ind. Appl.*, vol. 37, no. 4, pp. 1019–1027, Jul./Aug. 2001.

[12] M. Malinowski, M. Jasinski, and M. P. Kazmierkowski, "Simple direct power control of three-phase PWM rectifier using space-vector modulation (DPC-SVM)," *IEEE Trans. Ind. Electron.*, vol. 51, no. 2, pp. 447–454, Apr. 2004.

[13] T. Noguchi, H. Tomiki, S. Kondo, and I. Takahashi, "Direct power control of PWM converter without power-source voltage sensors," *IEEE Trans. Ind. Appl.*, vol. 34, no. 3, pp. 473–479, May/Jun. 1998.

[14] G. Escobar, A. M. Stankovic, J. M. Carrasco, E. Galvan, and R. Ortega, "Analysis and design of direct power control (DPC) for a three phase synchronous rectifier via output regulation subspaces," *IEEE Trans. Power Electron.*, vol. 18, no. 3, pp. 823–830, May 2003.

[15] J. Restrepo, J. Viola, J. M. Aller, and A. Bueno, "A simple switch selection state for SVM direct power control," in *Proc. IEEE Int. Symp. Ind. Electron. 2006*, Montreal, QC, Canada, Jul., vol. 2, pp. 1112–1116.

[16] P. Cortes, J. Rodriguez, D. E. Quevedo, and C. Silva, "Predictive current control strategy with imposed load current spectrum," *IEEE Trans. Power Electron.*, vol. 23, no. 2, pp. 612–618, Mar. 2008.

[17] P. Cortés, J. Rodríguez, P. Antoniewicz, and M. Kazmierkowski, "Direct power control of an AFE using predictive control," *IEEE Trans. Power Electron.*, vol. 23, no. 5, pp. 2516–2523, Sep. 2008.

[18] S. A. Larrinaga, M. A. R. Vidal, E. Oyarbide, and J. R. T. Apraiz, "Predictive control strategy for DC/AC converters based on direct power control," *IEEE Trans. Ind. Electron.*, vol. 54, no. 3, pp. 1261–1271, Jun. 2007.

[19] P. Antoniewicz, M. P. Kazmierkowski, S. Aurtenechea, and M. A. Rodriguez, "Comparative study of two predictive direct power control algorithms for three-phase AC/DC converters," in *Proc. IEEE Power Electron. Appl. 2007 Eur. Conf.*, Aalborg, Denmark, Sep., pp. 1–10.

[20] S. Vazquez, J. A. Sanchez, J. M. Carrasco, J. I. Leon, and E. Galvan, "A model-based direct power control for three-phase power converters," *IEEE Trans. Ind. Electron.*, vol. 55, no. 4, pp. 1647–1657, Apr. 2008.

[21] *IEEE Recommended Practices and Requirements for Harmonic Control in Electrical Power Systems*, IEEE Standard 519-1992, 1992.

[22] D. Xu, B. Feng, R. Li, K. Mino, and H. Umida, "A zero voltage switching SVM (ZVS-SVM) controlled three-phase boost rectifier," *IEEE Trans. Power Electron.*, vol. 22, no. 3, pp. 978–986, May 2007.

[23] Y. A. R. I. Mohamed and E. F. El-Saadany, "Robust high bandwidth discrete-time predictive current control with predictive internal model—A unified approach for voltage-source PWM converters," *IEEE Trans. Power Electron.*, vol. 23, no. 1, pp. 126–136, Jan. 2008.

[24] I. Takahashi and T. Noguchi, "A new quick-response and high-efficiency control strategy of an induction motor," *IEEE Trans. Ind. Appl.*, vol. 22, no. 5, pp. 820–827, Sep. 1986.

[25] M. Malinowski and M. P. Kamierkowski, "DSP implementation of direct power control with constant switching frequency for three-phase PWM rectifiers," in *Proc. IEEE 2002 28th Annu. Conf. Ind. Electron. Soc. (IECON'02)*, Nov., vol. 1, pp. 198–203.

[26] R. S. Herrera, P. Salmeron, and H. Kim, "Instantaneous reactive power theory applied to active power filter compensation: Different approaches, assessment, and experimental results," *IEEE Trans. Ind. Electron.*, vol. 55, no. 1, pp. 184–196, Jan. 2008.

[27] J. M. Aller, A. Bueno, J. A. Restrepo, M. I. Gimenez de Guzman, and V. M. Guzman, "Advantages of the instantaneous reactive power definitions in three phase system measurement," *IEEE Power Eng. Rev.*, vol. 19, no. 6, pp. 54–56, Jun. 1999.

[28] V. Soares, P. Verdelho, and G. D. Marques, "An instantaneous active and reactive current component method for active filters," *IEEE Trans. Power Electron.*, vol. 15, no. 4, pp. 660–669, Jul. 2000.

[29] J. M. Aller, A. Bueno, and T. Paga, "Power system analysis using space-vector transformation," *IEEE Trans. Power Syst.*, vol. 17, no. 4, pp. 957–965, Nov. 2002.

[30] G. Superti-Furga and G. Todeschini, "Discussion on instantaneous *p-q* strategies for control of active filters," *IEEE Trans. Power Electron.*, vol. 23, no. 4, pp. 1945–1955, Jul. 2008.

[31] J.-H. Youm and B.-H. Kwon, "An effective software implementation of the space-vector modulation," *IEEE Trans. Ind. Electron.*, vol. 46, no. 4, pp. 866–868, Aug. 1999.

[32] J. A. Restrepo, J. C. Viola, J. M. Aller, and A. Bueno, "Algorithm evaluation for the optimal selection of the space vector voltage using DPC in power systems," in *Proc. 2007 Eur. Conf. Power Electron. Appl.*, Aalborg, Denmark, Sep. 2007, pp. 1–9.

[33] J. Restrepo, J. M. Aller, J. Viola, and A. Bueno, "A simplified rectifier voltage vector selection for direct power control," in *Proc. 7th Int. Caribbean Conf. Devices, Circuits Syst. ICCDCS'08*, Cancun, Mexico, Apr., pp. 1–5.

Jose A. Restrepo (S'88–M'88) received the B.Sc. and M.Sc. degrees in electronics engineering from the Universidad Simón Bolívar, Caracas, Venezuela, in 1988 and 1991, respectively, and the Ph.D. degree from the University of Manchester Institute of Science and Technology, Manchester, U.K., in 1996.

He is currently a Full Professor of electronics engineering with the Departamento de Electrónica y Circuitos, Universidad Simón Bolívar. In 2002, he was a Visiting Professor with the School of Electrical and Computer Engineering, Georgia Institute of Technology, Atlanta. His current research interests include advanced control of electrical machines, artificial intelligence, power quality, and digital signal processors applied to motion control.

Jose M. Aller was born in Caracas, Venezuela, in 1958. He received the Eng. degree in electrical engineering from the Universidad Simón Bolívar, Caracas, in 1980, the M.S. degree in electrical engineering from the Universidad Central de Venezuela, Caracas, in 1982, and the Ph.D. degree in industrial engineering from the Universidad Politécnica de Madrid, Madrid, Spain, in 1993.

He has been a Lecturer at the Universidad Simón Bolívar for 28 years, where he is currently a Full-Time Professor in the Departamento de Conversión y Transporte de Energía teaching electrical machines and power electronics. He was the General Secretary of the Universidad Simón Bolívar from 2001 to 2005. He has been a Visiting Professor at the Georgia Institute of Technology, Atlanta, in 2000 and 2007. His current research interests include space-vector applications, electrical machine control, power electronics, and monitoring of electrical machines.

Julio C. Viola was born in La Paz (E.R.), Argentina, in 1975. He received the Electronics Engineering degree from the Universidad Tecnológica Nacional, Paraná (E.R.), Argentina, in 2000, and the Ph.D. degree from Universidad Simón Bolívar, Caracas, Venezuela, in 2008.

In 2005, he joined the faculty of Universidad Simón Bolívar, Caracas, Venezuela, as an Assistant Professor of electronics engineering. He became an Associate Professor in 2008. His current research interests include adaptive control of electrical machines using DSP and field-programmable gate array (FPGA), active power filters, and artificial intelligence.

Alexander Bueno was born in Caracas, Venezuela, in 1971. He received the Ing. and M.S. degrees in electrical engineering from Universidad Simón Bolívar, Caracas, in 1993 and 1997, respectively.

He has been a Lecturer at the Universidad Simón Bolívar for 16 years, where he is currently a Full-Time Professor in the Departamento de Conversión y Transporte de Energía teaching electrical machines and power electronics. His current research interests include space-vector control applications, electrical machines, neural network estimators, and power electronics.

Thomas G. Habetler (S'79–M'83–SM'92–F'02) received the B.S. and M.S. degrees in electrical engineering from Marquette University, Milwaukee, WI, in 1981 and 1984, respectively, and the Ph.D. degree from the University of Wisconsin, Madison, in 1989.

From 1983 to 1985, he was a Project Engineer with the Electro-Motive Division, General Motors. Since 1989, he has been with the School of Electrical and Computer Engineering, Georgia Institute of Technology, Atlanta, where he is currently a Professor of electrical engineering. He is a regular Consultant to industry in the field of condition-based diagnostics for electrical systems. His current research interests include electric machine protection and condition monitoring, switching converter technology, and drives. He has authored or coauthored over 150 papers in the field.

Dr. Habetler is the IEEE Division II Director-Elect, the Past-President of the IEEE Power Electronics Society, and the Past-Chair of the Industrial Power Converter Committee of the IEEE Industry Applications Society. He was the recipient of four conference prize paper awards from the IEEE Industry Applications Society.